Inorg. Chem. **2006**, *45*, 9901–9906

Absorption, Light Emission, and Upconversion Properties of Tm^{2+}-Doped $CsCaI_3$ and $RbCaI_3$

Eva Beurer, Judith Grimm, Pascal Gerner, and Hans U. GUdel*

Department of Chemistry and Biochemistry, University of Bern, Freiestrasse 3, 3012 Bern, Switzerland

Received July 19, 2006

Absorption, light emission, and upconversion properties of Tm^{2+}-doped $CsCaI_3$ and $RbCaI_3$ single crystals are presented and compared. Both compounds show multiple emissions after excitation at 21834 cm^{-1} between 10 and 300 K. Besides sharp 4f–4f transitions around 8800 cm^{-1}, five and three broad 4f–5d emission bands are observed at higher energies in $CsCaI_3$:Tm^{2+} and $RbCaI_3$:Tm^{2+}, respectively. The 4f–5d transitions are very sensitive to the crystalline environment: the onset of the 4f–5d excitations is red-shifted by about 1000 cm^{-1} in $RbCaI_3$:Tm^{2+} compared to $CsCaI_3$:Tm^{2+}. In addition, a broadening of bands is observed in the former compound. These differences are attributed to the structural changes that occur when the alkali metal is changed from Cs to Rb in these crystal lattices. An increased energy splitting of the multiplets and a red shift of the barycenter of the $(4f)^{12}$-$(5d)^1$ electron configuration in $RbCaI_3$:Tm^{2+} is the result. This affects not only the color of the visible emission, which turns from green in $CsCaI_3$:Tm^{2+} to yellow in $RbCaI_3$:Tm^{2+}, but also the excited state dynamics. As a consequence, the dominant upconversion processes are different in the two compounds. Thus, the two title compounds nicely illustrate the influence of the structural environment on the optical spectroscopic properties of Tm^{2+}.

1. Introduction

Light-emitting materials have numerous applications in everyday life. The wide range of applications ranging from laser welding to biolabeling requires diverse light-emitting materials with specific properties. The emission properties of luminescent dopant ions in spectroscopically inert host lattices can be influenced by variation of the chemical environment, the coordination environment, or the oxidation state. Lanthanides are frequently used as dopant ions, since they often show efficient luminescence from multiple excited states. Their most common oxidation state is the trivalent one, but Eu, Sm, Yb, and Tm can also be chemically stabilized in the divalent oxidation state in certain host lattices.[1−3] Tm^{2+} has 13 4f electrons in the ground state and is isoelectronic with Yb^{3+}. The 4f electrons in Tm^{2+} experience a reduced Coulomb attraction from the nucleus compared to those in Yb^{3+}. As a consequence, the lowest lying 4f−5d transitions in Tm^{2+} are located in the near-infrared (NIR) spectral region and are therefore spectroscopically easier accessible than those of Yb^{3+} situated above 60000 cm^{-1}.

Host lattices consisting of heavier halides are well suited to stabilize Tm in the divalent oxidation state. Early results on the optical spectroscopic properties of Tm^{2+} include the demonstration of laser oscillation on the intraconfigurational $^2F_{5/2} \leftrightarrow {}^2F_{7/2}$ transition in CaF_2:Tm^{2+} as one of the first lasing materials.[4] In addition, emission from the first 4f−5d state has been reported for Tm^{2+}-doped SrB_4O_7,[5] $SrCl_2$,[6] $BaZnCl_4$, and $SrZnCl_4$.[7] The light emission and absorption properties of $CsCaCl_3$:Tm^{2+} and $CsCaBr_3$:Tm^{2+} have recently been investigated.[8] In these hosts, Tm^{2+} shows up to four emission bands in the NIR and visible (VIS) spectral region originating in 4f−5d excited states, in addition to the 4f−4f emission in the NIR. The observation of multiple metastable 4f−5d states is remarkable and without precedent.

In some materials, VIS emission can be observed in a so-called upconversion (UC) process after excitation in the NIR.

* To whom correspondence should be addressed. E-mail: hans-ulrich.guedel@iac.unibe.ch.

(1) Blasse, G.; Grabmeier, B. C. *Luminescent Materials*; Springer-Verlag: Berlin, 1994.
(2) Rubio, J. *J. Phys. Chem. Solids* **1991**, *52*, 101.
(3) Grimm, J.; Güdel, H. U. *Chem. Phys. Lett.* **2005**, *404*, 40−43.
(4) Ducan, R. C.; Kiss, Z. J. *Appl. Phys. Lett.* **1963**, *3*.
(5) Schipper, W. J.; Meijerink, A.; Blasse, G. *J. Lumin.* **1994**, *62*.
(6) Wenger, O. S.; Wickleder, C.; Krämer, K. W.; Güdel, H. U. *J. Lumin.* **2001**, *94/95*, 101−105.
(7) Wickleder, C. *J. Alloys Compd.* **2000**, *300−301*.
(8) Grimm, J.; Suyver, J. F.; Beurer, E.; Carver, G.; Güdel, H. U. *J. Phys. Chem. B* **2006**, *110*, 2093−2101.

10.1021/ic061340+ CCC: $33.50
Published on Web 10/14/2006

At least two metastable states are required for this nonlinear optical process.[9] Due to their multiple emissions, the Tm^{2+}-doped halides are expected to undergo UC processes. The first UC studies on Tm^{2+}-doped $SrCl_2$ used $^2F_{5/2}$ as the intermediate state in a 4f to 5d UC process.[6] Recently, we reported a new type of NIR to VIS UC process in $CsCaX_3$:Tm^{2+} ($X = Cl^-$, Br^-, I^-), which exclusively involves 4f−5d excited states.[10] The 4f−5d transitions have a larger absorption cross-section than the 4f−4f transitions typically exploited in UC materials. The VIS/NIR photon ratio of 14.3% obtained for this UC process at 10 K is very high in $CsCaI_3$:Tm^{2+}.[11]

In contrast to the 4f−4f transitions, the 4f−5d transitions are strongly susceptible to changes coordination. $CsCaI_3$ and $RbCaI_3$ are both orthorhombically distorted perovskites. But the structures of the two crystal lattices are very different. In the present contribution, we investigate the influence of the structural differences on the absorption, light emission, and UC properties of $CsCaI_3$:Tm^{2+} and $RbCaI_3$:Tm^{2+}.

2. Experimental Section

2.1. Synthesis and Sample Preparation. Single crystals of nominally 0.5% and 1% Tm^{2+}-doped $CsCaI_3$ and $RbCaI_3$ were prepared from stoichiometric amounts of CaI and CsI or RbI, respectively, and Tm^{2+}, which was produced in situ by a synproportionation reaction of Tm metal (Alfa Aesar 99.9%) and TmI_3 (from 99.999% Tm_2O_3 from Johnson Matthey, prepared by the ammonium halide route[12]). All handling was done under inert atmosphere in a glovebox. The crystal growth by the Brigdeman technique was done in tantalum ampules to avoid oxidation of Tm^{2+} into Tm^{3+}. The obtained crystals have a size of up to 2 mm × 2 mm × 2 mm. The optical quality is good for $CsCaI_3$:Tm^{2+} and adequate for $RbCaI_3$:Tm^{2+}. The latter undergoes a phase transition at $T_C = 742$ K upon cooling the melt to room temperature,[13] and thus, the crystals were tempered for 120 h at 692 K to allow completion of the phase conversion. The phase of the crystals was confirmed by X-ray powder diffraction. To determine the absolute concentration of Tm, ICP−OES measurements were performed. The absolute concentrations are 0.76% in $CsCaI_3$:Tm^{2+} and 0.48% and 0.73% in $RbCaI_3$:Tm^{2+} for the crystals used in this paper.

Absorption measurements were carried out on polished crystals of $CsCaI_3$:Tm^{2+} (0.76%) and unpolished crystals of $RbCaI_3$:Tm^{2+} (0.48%) enclosed in an airtight copper cell with quartz windows using copper grease (Lake Shore cryotronics Inc.) to enable thermal contact. Emission measurements were performed on single crystals of $CsCaI_3$:Tm^{2+} (0.76%) and $RbCaI_3$:Tm^{2+} (0.73%) sealed into quartz ampules under He atmosphere.

2.2. Spectroscopic Measurements. For the absorption measurements, the samples were cooled with a closed-cycle cryostat (Air Products), and the spectra were recorded on a Cary 6000i spectrometer (Varian). Sample cooling for the luminescence measurements was achieved with the He gas flow technique. Photoexcitation of the emission spectra was done with the 457.9 nm line of an Ar^+ laser (Spectra Physics 2060-10 SA). For upconversion measurements, the samples were excited with a multimode standing wave Ti:sapphire laser (Spectra Physics 3900 S), pumped by the second harmonic of a Nd^{3+}:YVO_4 laser (Millenia Spectra Physics). The wavelength control of the Ti:sapphire laser was achieved by an inchworm-driven (Burleigh PPZ-501) birefringent filter and a wavemeter (Burleigh WA2100). The laser power was measured with a power meter (Coherent Labmaster Ultima), and the laser beam was focused using a $f = 53$ mm lens for the UC measurements. The typical excitation density used was 4.26 kW/cm^2 for UC experiments. For the two-color upconversion experiment, in addition to the Ti:sapphire laser, the output of a 280 W tungsten lamp (Thermo Oriel) was dispersed by a 1/4 m monochromator (MiniMate Spex) and focused onto the crystal (band-pass 40 nm). To measure the power dependence, a series of neutral density filters was used. Dispersion of the luminescence was achieved either with a 0.85 m double monochromator (Spex 1402) or a 0.75 m single monochromator (Spex 1702). The signal in the VIS was detected with a PMT (Hamamatsu P-3310-01) and a photon counting system (Stanford Research 400) or in the NIR range with a Ge detector (ADC 403HS) interfaced with a lock-in amplifier (Stanford Research 830). Either the Ar^+ laser chopped with an acousto-optic modulator (Coherent 305, Stanford Research DS 345 function generator), or the fundamental (1064 nm) or the third harmonic (355 nm) of a pulsed Nd:YAG laser (Quanta Ray DCR 3, 20 Hz) was used to measure luminescence transients. Transient signals were detected as described above using a multichannel scaler (Stanford Research 430) or an oscilloscope (Tektronix TDS 540a). The luminescence spectra are displayed as photon counts versus energy and are corrected for the sensitivity of the detection system.[14]

4. Results and Discussion

4.1. Structure and Site Symmetry. $CsCaI_3$ and $RbCaI_3$ crystallize in the orthorhombic *Pbnm* (No. 62) space group.[15] In $CsCaI_3$, the CaI_6^{4-} units are arranged as corner-sharing octahedra in the orthorhombically distorted perovskite structure, while they form a double-chain structure consisting of edge-sharing octahedra in $RbCaI_3$. The distance between nearest-neighbor Ca^{2+} sites is 6.08 Å in $CsCaI_3$. In $RbCaI_3$ it is 4.503 Å between the two chains of the ladder and 4.666 Å along the chains.

Tm^{2+} replaces Ca^{2+} on a distorted octahedral site in both structures. The distortion from O_h symmetry is expressed by the deviation of the octahedral angles from 90° and by the variation of the metal−ligand bond lengths. The deviation of the octahedral angles in $CsCaI_3$ ranges from 0.08° to 1.14°, and the variation of the $Ca^{2+}-I^-$ bond length is within 0.02 Å. In $RbCaI_3$ the angles deviate between 1.28° and 5.46° from 90°, and the variation of the bond lengths is within 0.1 Å. The average metal−ligand bond length is bigger in $RbCaI_3$:Tm^{2+} (3.13 Å) than in $CsCaI_3$:Tm^{2+} (3.09 Å). The Ca^{2+} site symmetries are C_i and C_s in $CsCaI_3$ and in $RbCaI_3$, respectively.

4.2. 4f−4f Excitations. The $^2F_{7/2} \leftrightarrow {}^2F_{5/2}$ transitions of Tm^{2+} are observed in absorption and emission after 21834 cm^{-1} excitation around 8800 cm^{-1}. The 10 K spectra are

(9) Suyver, J. F.; Aebischer, A.; Biner, D.; Gerner, P.; Grimm, J.; Heer, S.; Krämer, K.; Reinhard, C.; Güdel, H. U. *Opt. Mater.* **2005**, *27*, 1111−1130.
(10) Grimm, J.; Beurer, E.; Gerner, P.; Güdel, H. U. *Chem. Eur. J.*, submitted.
(11) Beurer, E.; Grimm, J.; Gerner, P.; Güdel, H. U. *J. Am. Chem. Soc.* **2006**, *128*, 3110−3111.
(12) Meyer, G. *Adv. Synth. React. Solids* **1994**, *2*.
(13) Seifert, H. J.; Mueller, B.; Stoezel, E. *Rev. Chim. Miner.* **1980**, *17*, 147−157.
(14) Ejder, E. *J. Opt. Soc. Am.* **1969**, *59*.
(15) Schilling, G.; Meyer, G. *Z. Anorg. Allg. Chem.* **1996**, *622*, 759−765.

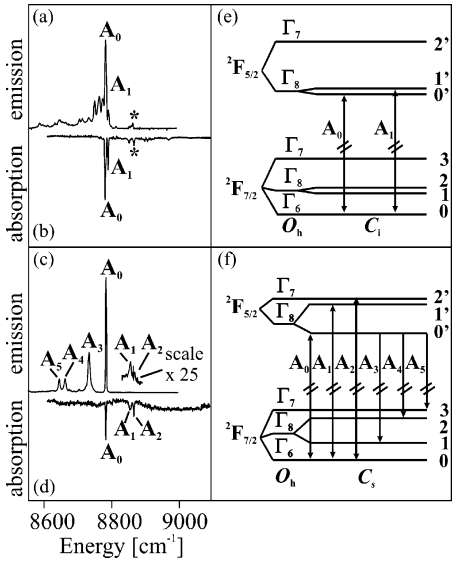

Figure 1. (a, c) $^2F_{5/2} \leftrightarrow {}^2F_{7/2}$ emission and (b, d) absorption spectra of Tm^{2+}-doped $CsCaI_3$ and $RbCaI_3$, respectively, measured at 10 K. Excitation of the emission spectra occurred at 21834 cm^{-1}. In parts e and f, the schematic crystal-field (CF) splittings of the $^2F_{7/2}$ and $^2F_{5/2}$ multiplets are shown for $CsCaI_3$:Tm^{2+} and $RbCaI_3$:Tm^{2+}, respectively.

Table 1. Positions of the Crystal-Field Levels of the $^2F_{7/2}$ and $^2F_{5/2}$ Multiplets of Tm^{2+}-Doped $CsCaI_3$ and $RbCaI_3$[a]

compd	multiplet	spinor	position [cm^{-1}]
$CsCaI_3$:Tm^{2+}	$^2F_{7/2}$	0	0
	$^2F_{5/2}$	0	8782
		1	8790
$RbCaI_3$:Tm^{2+}	$^2F_{7/2}$	0	0
		1	51
		2	122
		3	139
	$^2F_{5/2}$	0	8783
		1	8854
		2	8866

[a] The levels are labeled as in Figure 1.

displayed in Figure 1a,b and Figure 1c,d for $CsCaI_3$:Tm^{2+} and $RbCaI_3$:Tm^{2+}, respectively. Little structure is observed in the absorption spectra (Figure 1b,d). The dissimilarity between the emission spectra (Figure 1a,c) is striking. In $CsCaI_3$:Tm^{2+}, the $^2F_{7/2} \leftrightarrow {}^2F_{5/2}$ transitions are electric-dipole (ED) forbidden. The transitions labeled A_0 and A_1 are assigned to electronic origins (Figure 1e), since their emission and absorption lines coincide. They arise by a magnetic dipole (MD) mechanism. Their energy difference of 8 cm^{-1} represents the splitting of the $^2F_{5/2}(\Gamma_8)$ due the symmetry reduction from O_h to C_i. Further origins cannot be assigned. In emission, the remaining origins are most likely hidden by the vibronic sidebands of $CsCaI_3$:Tm^{2+}. In absorption, the electronic origin $^2F_{7/2}(\Gamma_6) \rightarrow {}^2F_{5/2}(\Gamma_7)$ is not observed because it is both ED and MD forbidden. The energy positions of the crystal-field levels are given in Table 1. The absorption and emission lines labeled with an asterisk are assigned to transitions on a minority Tm^{2+} site due to their different temperature dependence.

In contrast to $CsCaI_3$:Tm^{2+}, the center of inversion is lacking in the $RbCaI_3$:Tm^{2+} structure, and the 4f−4f origins are expected to have intensity. The absorption and emission spectra of $RbCaI_3$:Tm^{2+} in the region of the 4f−4f transitions

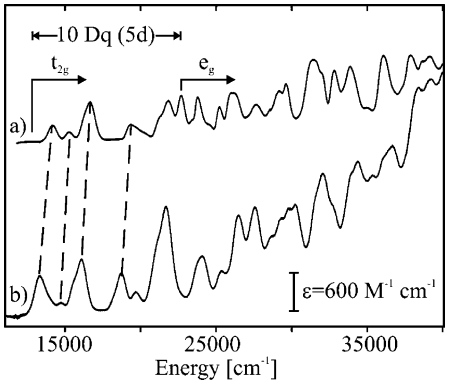

Figure 2. Absorption spectra of (a) $CsCaI_3$ and (b) $RbCaI_3$ doped with Tm^{2+}. The dotted lines connect corresponding bands in the two spectra. The onset of the t_{2g} and e_g absorption sets are indicated on top of the absorption spectrum of $CsCaI_3$:Tm^{2+}.

consist of several well-resolved sharp bands, see Figure 1c,d. A full analysis of the crystal-field levels of the $^2F_{7/2}$ and $^2F_{5/2}$ multiplet is thus possible, see Figure 1f. The energy positions are also listed in Table 1. The splitting of the octahedral Γ_8 states resulting from the increased distortion of the Tm^{2+} site is much bigger in $RbCaI_3$:Tm^{2+} than in $CsCaI_3$:Tm^{2+}. The total crystal-field splittings of the $^2F_{7/2}$ and the $^2F_{5/2}$ multiplets in $RbCaI_3$:Tm^{2+} appear reasonable for an iodide.[16,17]

4.3. 4f−5d Excitations. In Figure 2, the absorption spectra in the region of the 4f−5d excitations up to 40000 cm^{-1} are shown. The bands are broad and intense, which is expected for parity allowed 4f−5d transitions. Up to 22300 cm^{-1}, similar band shapes are observed in the two crystals, although they are shifted by about 1000 cm^{-1} to lower energies in $RbCaI_3$:Tm^{2+}. This shift arises from the energy difference between the $(4f)^{13}$ and the $(4f)^{12}(5d)^1$ barycenters, which is determined by several interactions such as the polarizability of the ligands and covalency.[18] The covalency is smaller in $RbCaI_3$:Tm^{2+} because of the bigger metal−ligand distance. A reduced covalency will induce a shift of the $(4f)^{12}(5d)^1$ barycenter toward lower energies, which is observed in the spectra.

One of the interactions lifting the degeneracy in the $(4f)^{12}(5d)^1$ electron configuration is the crystal-field splitting of the 5d electron, giving rise to t_{2g} and e_g sets with an energy difference of 10*Dq*. In octahedral coordination, the t_{2g} sets lies lower in energy. In $CsCaI_3$:Tm^{2+} we can recognize the onset of the $(4f)^{12}e_g$ excitations and thus estimate $10Dq = 8500$ cm^{-1}, as indicated in Figure 2.[19] A slightly reduced value is expected in $RbCaI_3$:Tm^{2+}, but it cannot be assigned unambiguously in the spectrum. Above 22300 cm^{-1} the similarity of the two absorption spectra is not continued.

The t_{2g} and e_g orbitals are further split because of the distorted octahedral sites. The stronger distortion in the $RbCaI_3$:Tm^{2+} manifests itself in a broadening of the absorption bands by about 300 cm^{-1}, see Figure 2. For simplicity

(16) Tanner, P. *Mol. Phys.* **1986**, *58*, 317−328.
(17) Hehlen, M. P.; Güdel, H. U. *J. Chem. Phys.* **1993**, *98*, 1768−1775.
(18) Andriesen, J.; Dorenbos, P.; van Eijk, C. W. E. *Phys. Rev. B* **2005**, *72*, 045129.
(19) Grimm, J.; Beurer, E.; Güdel, H. U. *Inorg. Chem.*, accepted.

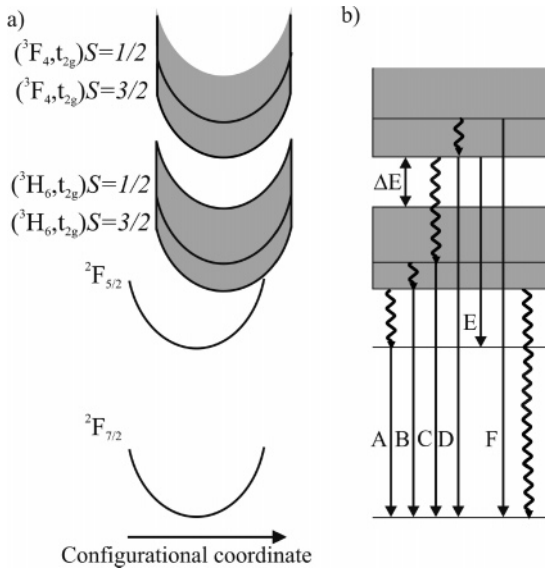

Figure 3. (a) Schematic single-configurational coordinate (SCC) diagram of Tm^{2+}-doped $CsCaI_3$ assuming harmonic potentials and equal force constants for all the states. In part b, the diagram is shown without the SCC. Radiative and nonradiative relaxation processes are represented by straight and curly arrows, respectively. The labels are defined in the text. ΔE is the important energy gap between the ($^3H_6$, t_{2g}) and ($^3F_4$, t_{2g}) multiplets.

we keep the O_h notation for labeling of the multiplets. Spin−orbit coupling and Coulomb repulsion within the $4f^{12}$ electron configuration lead to Tm^{3+}-like $^{2S+1}L_J$ terms that are coupled to t_{2g} and e_g. In addition, exchange interactions between the 4f and 5d electrons split the multiplets into a high-spin ($S = {}^3/_2$) and a low-spin ($S = {}^1/_2$) set. The spectroscopically relevant states arising from these interactions are shown for the low-energy multiplets in Figure 3a in a schematic single-configurational coordinate diagram.

Figure 4a,c shows the 10 K emission spectra of $CsCaI_3$:Tm^{2+} and $RbCaI_3$:Tm^{2+}, respectively, after laser excitation at 21834 cm^{-1}. The emission bands are labeled A−F. The emission bands B, C, and D of Tm^{2+} are shifted to lower energies by about 1000 cm^{-1} in $RbCaI_3$:Tm^{2+} compared to $CsCaI_3$:Tm^{2+}. In Figure 4b,d the onsets of the corresponding 10 K absorption spectra are shown upside down. The absorption bands are labeled as in Figure 3b. The lowest 4f−5d absorption bands are very weak. They are marked with an arrow in Figure 4 and assigned to "spin-forbidden" transitions from the $^2F_{7/2}$ ground state into the high-spin ($^3H_6$,t_{2g}) $S = {}^3/_2$ set of levels (Figure 3a).[20] Emission B is observed from this multiplet (Figure 4a,c). The lowest "spin-allowed" absorption with a higher absorption cross section is also marked with an arrow in Figure 4 and occurs into the ($^3H_6$,t_{2g}) $S = {}^1/_2$ multiplet. Emission C (Figure 4a,c) corresponds to a transition from the lowest lying component of the ($^3H_6$,t_{2g}) $S = {}^1/_2$ into the groundstate. The emissions D and F originate in the higher excited ($^3F_4$,t_{2g}) multiplet. E is the interexcited-state emission from the ($^3F_4$,t_{2g}) to $^2F_{5/2}$. In $RbCaI_3$:Tm^{2+}, emissions E and F are not observed. While

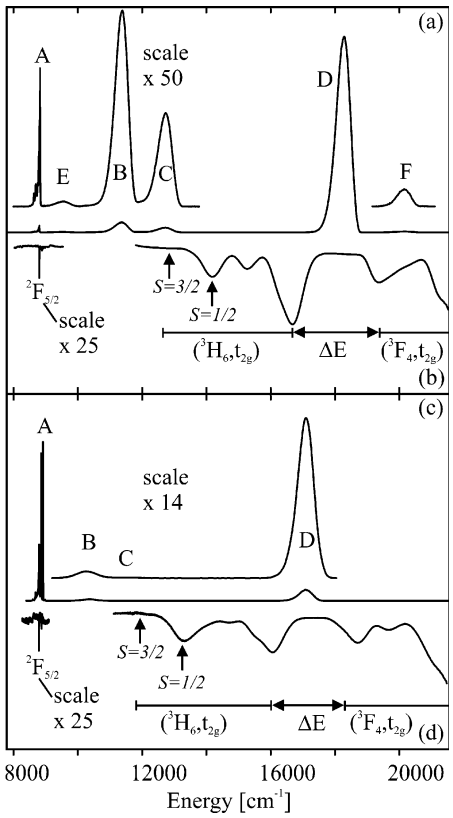

Figure 4. Single crystal (a) emission and (b) absorption (upside down) spectrum of $CsCaI_3$:Tm^{2+} recorded at 10 K. In parts c and d, the same data are presented for $RbCaI_3$:Tm^{2+}. Photoexcitation of the emission spectra occurred at 21834 cm^{-1}. Note the scaling factors for the various emission and absorption bands. The labels of the absorption and emission bands are explained in the text. ΔE is the energy gap defined in Figure 3.

Table 2. Percentage of the Totally Emitted Photons in Each Emission Band under Downconversion and Upconversion Excitation at 10 K and the Position of the Emission Bands[a]

compd	emission	integrated photon counts [%] DC	integrated photon counts [%] UC	position [cm^{-1}]
$CsCaI_3$:Tm^{2+}	A	0.3	0.02	8782
	B	4.6	87.23	11350
	C	2.3	0.12	12700
	D	92.3	12.49	18280
	E	0.1		9500
	F	0.4	0.15	20150
$RbCaI_3$:Tm^{2+}	A	72.9	91.4	8783
	B	3.5	4.5	10300
	C	0.2		11680
	D	23.4	4.1	17120

[a] The DC luminescence was excited at 21834 cm^{-1} whereas the UC was induced exciting at 12350 cm^{-1} in $CsCaI_3$:Tm^{2+} and 12050 cm^{-1} in $RbCaI_3$:Tm^{2+} with a laser power density of 4.26 kW/cm^{-1}.

emission D is green in $CsCaI_3$:Tm^{2+}, it appears yellow in $RbCaI_3$:Tm^{2+}.

4.4. Emission Dynamics and Temperature Dependence. The distribution of photons among the emission bands at 10 K upon excitation at 21834 cm^{-1} is very different for $CsCaI_3$:Tm^{2+} and $RbCaI_3$:Tm^{2+} (see Figure 4 and Table 2). While the dominant emission in $CsCaI_3$:Tm^{2+} is emission D in the VIS, emission A in the NIR is most prominent in $RbCaI_3$:Tm^{2+}. At first sight this is astonishing, since in both hosts the phonon energy is low and the absorption spectra look

(20) McClure, D. S.; Kiss, Z. J. *J. Chem. Phys.* **1963**, *39*, 3251.
(21) Gerner, P.; Wenger, O. S.; Valiente, R.; Güdel, H. U. *Inorg. Chem.* **2001**, *40*, 4534.

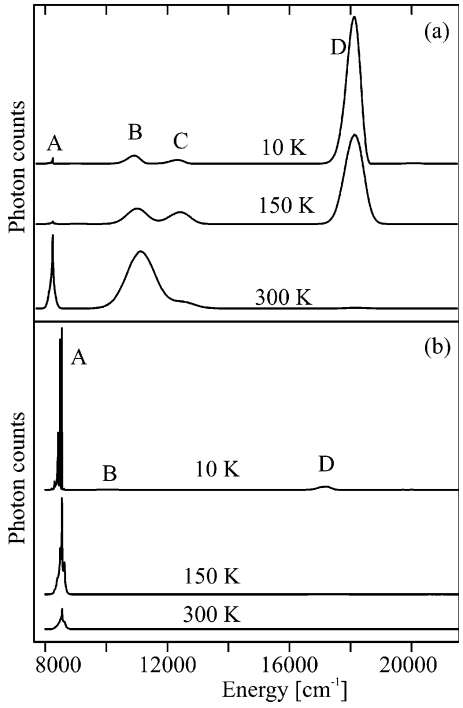

Figure 5. Emission spectra of Tm^{2+}-doped (a) $CsCaI_3$ and (b) $RbCaI_3$ at 10, 150, and 300 K. The emission was photoexcited at 21834 cm^{-1}. The spectra are shifted arbitrarily along the vertical axis and are normalized within part a or b.

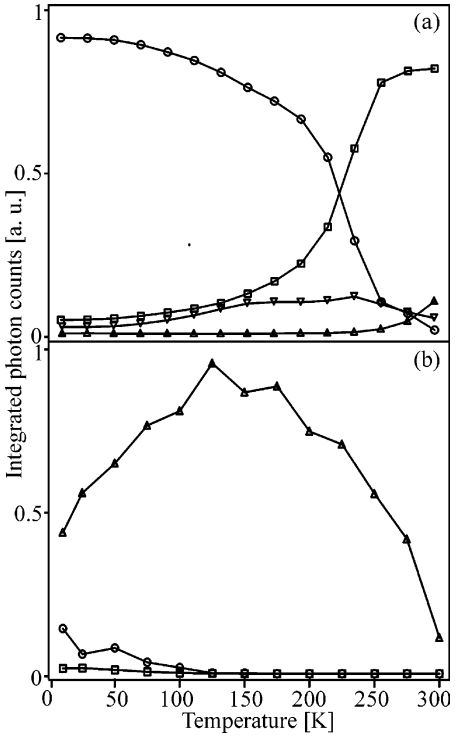

Figure 6. Temperature dependence of the integrated photon counts (normalized to a total of 1) of the dominant emissions of Tm^{2+} in (a) $CsCaI_3$ and (b)$RbCaI_3$: △, transition A; □, transition B; ▽, transition C; O, transition D. The solid lines are a guide to the eye. The photon counts were corrected for the decreasing absorption cross section at the excitation energy of 21834 cm^{-1}.

similar (Figure 4). The key to this difference is the energy gap ΔE separating the lowest level of the ($^3F_4$,t_{2g}) multiplet from the highest level of ($^3H_6$,t_{2g}). This is significantly smaller in $RbCaI_3$:Tm^{2+} (Figures 3 and 4), and thus, the multiphonon relaxation across ΔE in this lattice is more efficient. As a result of the redshift by about 1000 cm^{-1} of the lowest 4f−5d absorptions, also the energy gap between ($^3H_6$,t_{2g}) and $^2F_{5/2}$ is significantly reduced in $RbCaI_3$:Tm^{2+}. The concomitant increase of the nonradiative relaxation rate leads to the dominance of emission A already at 10 K.

Figure 5 shows emission spectra of the two samples, both excited at 21834 cm^{-1}, at 10, 150, and 300 K. Also, Figure 6 contains plots of the temperature dependence of the integrated photon counts of the most prominent emission bands in Tm^{2+}-doped $CsCaI_3$ and $RbCaI_3$. Again, the behavior of the two samples is completely different. In $CsCaI_3$:Tm^{2+}, emission D is dominant up to 230 K. At higher temperatures, multiphonon relaxation from ($^3F_4$,t_{2g}) to ($^3H_6$,t_{2g}) becomes competitive. At room temperature, the intensity of D is low, although not completely quenched and still observable by eye. The decrease of emission D is accompanied by an increase of the intensity of emission B, which remains the dominant emission up to 300 K in $CsCaI_3$:Tm^{2+}. Multiphonon relaxation processes from ($^3H_6$,t_{2g}) to $^2F_{5/2}$ set in with increasing temperature, but at 300 K emission A is still a factor of 8 lower than emission B. The intensities of emissions E and F remain low over the whole temperature range.

In $RbCaI_3$:Tm^{2+}, emission A strongly dominates the spectrum at all temperatures. Above 125 K, emissions B, C, and D are quenched completely. Above 150 K the quantum efficiency of emission A starts to decrease. This indicates that at elevated temperatures a nonradiative decay mechanism from the 4f−5d excited states to the ground state becomes operative. Multiphonon processes between the 4f states cannot account for this loss, because the gap between the $^2F_{5/2}$ and the $^2F_{7/2}$ is too large to be bridged by phonons for a Huang−Rhys factor close to zero.

4.5. Upconversion Emission. In Figure 7a,b, the 10 K emission spectra of $CsCaI_3$:Tm^{2+} excited at 12350 cm^{-1} and of $RbCaI_3$:Tm^{2+} excited at 12050 cm^{-1} in the NIR are shown. Multiple emissions are observed in both samples after this excitation into the ($^3H_6$,t_{2g}) $S = {}^3/_2$ multiplet. The samples are excited with the same laser power density of approximately 4.26 kW/cm^2, and the same notation of emission bands as in Figure 4 is used. The observation of emission D in the visible part of the spectrum clearly indicates an upconversion (UC) process in both samples at 10 K.

In $CsCaI_3$:Tm^{2+}, the UC process consists of a 4f−5d excitation followed by a 5d(t_{2g})−5d(e_g) excitation as schematically shown in Figure 7. After a ground-state absorption step (GSA), the second step of the UC process can occur either by excited-state absorption (ESA) or by energy transfer upconversion (ETU). In $CsCaI_3$:Tm^{2+} both UC mechanisms occur simultaneously.[10] The dominant UC process taking place in $RbCaI_3$:Tm^{2+} is different, see Figure 7d. The originally excited ($^3H_6$,t_{2g}) $S = {}^3/_2$ multiplet efficiently relaxes to $^2F_{5/2}$, from where a 4f−5d ESA step leads up to ($^3F_4$,t_{2g}).

The VIS/NIR photon ratio at 10 K in $CsCaI_3$:Tm^{2+} is 14.3% for a laser power density of 4.26 kW/cm^{-1} (Figure 7a). This is a surprisingly high value, comparable to trivalent

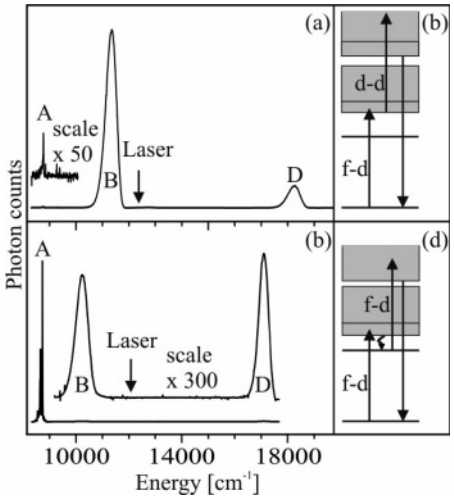

Figure 7. Upconversion emission spectrum of (a) $CsCaI_3:Tm^{2+}$ and (b) $RbCaI_3:Tm^{2+}$ at 10 K. In parts c and d, the corresponding energy level diagrams with the dominant UC processes are shown. Straight arrows represent radiative transitions, whereas the curly arrow indicates a multiphonon relaxation process. Photoexcitation with a power density of 4.26 kW/cm^{-1} occurred at 12350 cm^{-1} for $CsCaI_3:Tm^{2+}$ and at 12050 cm^{-1} for $RbCaI_3:Tm^{2+}$ and is indicated by an arrow in the spectra. Note the scaling factors for the various emission bands.

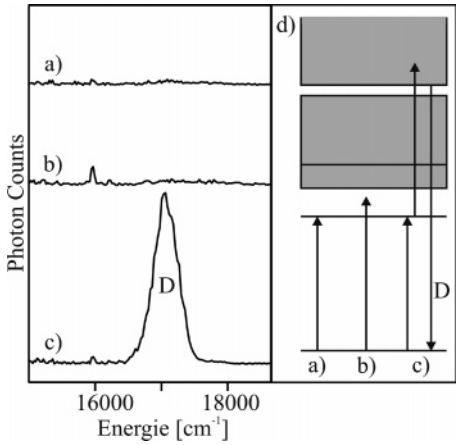

Figure 8. The 10 K UC emission spectrum of $RbCaI_3:Tm^{2+}$ is shown upon (a) lamp excitation around 8800 cm^{-1} (few microwatts), (b) laser excitation at 10275 cm^{-1} (100 mW), and (c) simultaneous lamp and laser excitation. The energy level diagram in part d schematically illustrates the processes in situations a−c.

lanthanide upconversion systems.[9] We ascribe this to a sequence of relatively intense absorption steps (4f−5d followed by 5d−5d, see Figure 7b) and the long lifetimes of both the intermediate ($^3H_6$,t_{2g}) $S = {}^3/_2$ and the emitting ($^3F_4$,t_{2g}) states. For the same NIR power density the VIS/NIR ratio in $RbCaI_3:Tm^{2+}$ is only 4.3%. This is surprising at first, because in this material, UC arises from a sequence of two intense 4f−5d excitations (see Figure 7d), and we expect a high UC efficiency. The reduced VIS/NIR photon ratio results from a loss process already discussed in section 4.4. The energy gap ΔE between the ($^3F_4$,t_{2g}) and ($^3H_6$,t_{2g}) multiplets (see Figure 3b) is strongly reduced compared to $CsCaI_3:Tm^{2+}$, and multiphonon relaxation across this gap is efficient. Thus, even though the UC process itself is probably more efficient in $RbCaI_3:Tm^{2+}$ than in $CsCaI_3:Tm^{2+}$, the observed VIS/NIR ratio is smaller due to this nonradiative relaxation.

To prove that UC can be induced from the $^2F_{5/2}$ as the intermediate excited state, a two-color UC experiment was performed in $RbCaI_3:Tm^{2+}$ by using two light sources with different excitation wavelengths. Figure 8a−c shows the 10 K two-color UC luminescence spectra of $RbCaI_3:Tm^{2+}$. Direct excitation into the $^2F_{5/2}$ at 8800 cm^{-1} was achieved by a tungsten lamp using a monochromator and filters to select the excitation energy, and for the ESA step into the ($^3F_4$,t_{2g}) multiplet a Ti:sapphire laser at 10250 cm^{-1} was used. The latter excitation corresponds to an energy below the onset of the 4f−5d ground-state absorption. Neither the lamp itself nor the laser itself are able to induce UC emission (Figure 8a,b, respectively). A combination of both excitation sources, however, produces emission D as a distinct UC signal shown in Figure 8c. The excitation schemes for the three experiments are indicated in Figure 8d. The efficiency of the ESA step in this UC process must be very high, since the excitation power of the lamp was in the order of a few microwatts, and nevertheless a good detectable UC signal is observed.

5. Conclusions

The small chemical variation between $CsCaI_3:Tm^{2+}$ and $RbCaI_3:Tm^{2+}$ has drastic effects on the light emission properties. A relatively modest distortion of the TmI_6 coordination octahedron in $RbCaI_3:Tm^{2+}$ is found to be responsible for this. Its main effect is to reduce the relevant energy gaps between excited states and thus affect the competition between radiative and nonradiative relaxation processes.

Designing a material, which combines the low multiphonon rate constant from ($^3F_4$,t_{2g}) found in $CsCaI_3:Tm^{2+}$ with the efficient UC process in $RbCaI_3:Tm^{2+}$, would possibly lead to an extraordinarily efficient UC phosphor. This would require a smaller distortion of the coordination octahedron than in $RbCaI_3:Tm^{2+}$ to avoid the reduction of the energy gap ΔE. On the other hand, the barycenter of the $(4f)^{12}(5d)^1$ states should be at low energy such as in $RbCaI_3:Tm^{2+}$, to enable efficient nonradiative relaxation into the $^2F_{5/2}$. A possibility might be to synthesize mixed crystals of Tm^{2+}-doped $RbCaI_3$ and $CsCaI_3$ and hopefully tune the energy gaps to an optimal value.

Acknowledgment. The Swiss National Science Foundation is gratefully acknowledged for financial support.

IC061340+